A Mechanical Amplifier for Haptic Feedback

Jack Lindsay

A thesis
submitted in partial fulfillment of the
requirements for the degree of

Master of Science in Engineering

University of Washington

2013

Committee:

Blake Hannaford, Chair

Per Reinhall

Brian Fabien

Program Authorized to Offer Degree:
Mechanical Engineering

University of Washington

Abstract

A Mechanical Amplifier
for Haptic Feedback

Jack Lindsay

Chair of the Supervisory Committee:
Professor Blake Hannaford
Electrical Engineering

Vibrotactile devices suffer from poor energy efficiency, arising from a mismatch between the device and the impedance of the human skin. This results in over-sized motors and excessive power consumption, and prevents development of more sophisticated, miniaturized and low-power mobile tactile devices. Herein, I investigate the feasibility of improving the energy transfer by placing a passive amplifier between the skin and the motor, dubbed an impedance adapter. I simulate the effects of this impedance adapter using a mathematical model, and evaluate its effect on skin displacement and a parameter I call skin stimulus. Skin stimulus is introduced as a measure of the perceptive effects of a haptic system, and is used to compare results between systems with an impedance adapter and those without. Functional prototypes are constructioned, and the design is experimentally verified. This system is able to quadruple the motion of the skin without increasing power consumption, and produce sensations equivalent to a standard system while consuming 1/2 of the power. By greatly reducing the size and power constraints of vibration motors, this technology offers a means to realize more sophisticated, smaller haptic devices.

TABLE OF CONTENTS

Page

List of Figures iii

List of Tables v

Chapter 1: Introduction 1
1.1 Theory of Operation 5

Chapter 2: Simulation and Optimization 7
2.1 Methods 7
2.1.1 Model 7
2.2 Simulation Results 13
2.2.1 Initial Simulation 13
2.2.2 Optimization for skin displacement 14
2.2.3 Skin Stimulus 14
2.3 Simulation Discussion 18

Chapter 3: Prototyping and Experimental Validation 22
3.1 Skin Displacement 23
3.1.1 Experiment 23
3.1.2 Results 24
3.2 Equivalent Perception 26
3.2.1 Experiment 26
3.2.2 Results 27
3.3 Discussion 28

Chapter 4: Conclusion 30
4.1 Future Work 30

Bibliography 33

LIST OF FIGURES

Figure Number Page

2.1 Dynamic model of vibrotactile actuator coupled to skin with an impedance adapter. Skin parameters depend on many variables including contact area (see text). 8

2.2 Receptive fields on the fingerpad. The blue cicle represents a contactor of radius 2, the red circles represent those receptors directly stimulated, and the grey circles are those unaffected. 13

2.3 Simulated skin displacement over time. The system with an impedance adapter has a much longer rise time, but achieves an amplitude approximately four times greater than the system without. 15

2.4 Impedance of the skin and impedance of the LRA + impedance adapter over a range of frequencies. The impedance adapter creates a dip in impedance right at the operating frequency, matching the impedance of the skin. 16

2.5 Sensitivity of RMS displacement output to changes in the impedance adapter and the skin model parameters. K_a impedance adapter stiffness; B_s skin damping; M_{a2} mass at skin contact. X-axis: percent change from optimal parameter value, Y-axis: relative steady state RMS displacement. 17

2.6 Number of receptors stimulated (N_r) as a function of contactor area. 18

2.7 Skin Stimulus as a function of contactor radius. The rough contours of the graph are an artifact of simulation due to a simplified distribution of skin receptors. 19

3.1 Schematic diagram of an impedance adapter and LRA. The finger is placed through the loop of the elastic band. 23

3.2 The prototype impedance adapter in test setup for displacement measurement. 25

3.3 (A) RMS skin displacement for a contactor with a radius of 4.5mm. (B) RMS skin displacement for a contactor with a radius of 1mm 26

3.4 Subjects adjust voltage levels on an LRA on one index finger to match the vibration sensed from an LRA on the other index finger. (A) Shows tests with a large radius, (B) shows tests with a smaller radius. 27

3.5 Linearity of the LRA and impedance adapter at power levels. 28

LIST OF TABLES

Table Number Page

2.1 Model Parameters 10
2.2 Parameter search ranges for the impedance adapter parameters. 11
2.3 Steady state RMS displacement with sinusoidal 5V input under three contact conditions. 12
2.4 Optimized impedance adapter parameters. Values marked with * were saturated at their lower search bound. 15

Chapter 1

INTRODUCTION

Vibration motors are used ubiquitously for haptic feedback – they are built into every smartphone and modern game controller and are used for everything from notification to tactile feedback. Most vibration motors produce vibration by accelerating a mass back and forth at high frequency. These motors offer a simple means of conveying tactile cues to users, and can be built into large arrays for more sophisticated haptic rendering [22, 10] However, the perceptibility of haptic sensations is limited by the size of the vibrating mass, and consequently, the power consumption required to move that mass. This means that miniaturized haptic feedback systems and power-limited mobile devices can only produce a fraction of the possible haptic sensations afforded by vibration motors.

Overcoming these limitations requires shrinking motors and cutting power consumption. Unfortunately, vibrotactile devices are fundamentally constrained by the skins vibrotactile threshold, or the threshold below which vibrations are imperceptible. Surpassing the vibrotactile threshold places constraints on the minimum size of the motor mass and its acceleration. Moreover, as the number of motors and vibration levels increases, these systems require even more power and space. Because of the relationship between perception, vibration, and power, researchers have recently attempted to maximize transmission of energy from the motor to the skin.

For instance, Jiang et al. use an elastic support structure to manage the load to the motor [10] and increase skin displacement. This system is appropriate for applications like lower leg prosthetics, but is not suitable for tactile stimulation of the hands and fingers in mobile devices because the system requires a large surrounding structure.

In this thesis, I investigate whether or not it is possible to improve the transmission of

energy from the device to the skin by introducing a medium between the skin and the motor. This medium works by coupling the output of the vibration motor to the impedance of human skin. For this purpose, I dub the medium an impedance adapter. How will changes in the characteristics of an impedance adapter have an effect on the deformation of skin? The skin is highly non-linear, and its elasticity shows a non-linear dependence on contact area [20], indentation [6], frequency [13], and location on the body [12]. Practical design constraints make it impossible for a given tactile device to be optimized over all of these variables. However, a simple device placed between the actuator and the skin contact point might effectively match the impedance between the load and source to maximize the power transfer. The efficacy of this device can be measured by its effect on signal amplitude, in this case the stimulus delivered to the skin, and its latency, or the time delay between the signals transmission and its maximum steady-state value.

This thesis investigates how an impedance adapter can be tuned to maximize skin deformation in a system driven by a particular class of vibrational motor, a linear resonant actuator (LRA). Furthermore, it considers how variations in the skin model will influence deformation. The LRA was chosen for its low latency and positive response to increases in mass [14]; as well as its low-cost, wide availability, and extensive use in the marketplace. Linear resonant actuators use a voice coil to generate an electrodynamic force between an outer housing and a permanent magnet-mass riding on a spring suspension. By oscillating the electric field, the inner mass vibrates at an amplitude that is a function of the excitation frequency. Maximum amplitude is acheived when the field excitation matches the resonant frequency of the mechanical spring-mass system. An LRA can be designed to produce either normal or tangential displacements, depending on the orientation of the mass and spring. Work by [3] found that the fingerpad is more sensitive to normal forces than tangential forces, as a result of the nearly five-fold greater stiffness in the tangential direction. Therefore systems working on the fingerpad and limited by peak force will see the best results with stimulation normal to the finger[3]. Because we aim to maximize stimulus to the fingerpad, only normal forces are considered in this study.

Skin's mechanical impedance depends on contact area, location on the body, frequency, and direction of displacement. In particular, these parameters influence the reactance, or the contribution of the mass and elasticity. Franke [5] found mass to dominate elasticity over 50 Hz on the thigh, and found it increases with the third power of the contactor diameter. Moore and Mundy [13] found that mass dominates in the range of 130 Hz on the finger pad, and elasticity dominates above 250 Hz or below 80 Hz for a range of contactor areas while damping was nearly constant over the range of frequencies. Wiertlewski and Hayward [21] found stiffness, damping, and mass to follow a roughly 1/3 power law of contactor area on the fingertip when a tangential force was applied, and described the fingertip as a visco-elastic medium with a corner frequency around 100 Hz, above which damping dominated. Lundstrom [12] also found the damping to be nearly constant, both over a range of frequencies and over the surface of the human hand when a normal displacement was applied. Values for stiffness and damping varied widely from study to study, and variation appears to depend on probe area, depth of indentation, frequency, and subject to subject variation [15, 12, 13, 5, 3]. While the lack of consensus in these findings presents challenges for modeling and simulation, I have endeavored to employ the best data available, and make the process transparent such that future work might improve upon our model.

A mechanical model of the human finger does not directly predict the stimulus provided by a haptic device. Previous studies have attempted to quantify the effect of contactor area on "skin stimulus", defined as displacement multiplied by area [14]. These results were based on data taken from the thigh, and cannot be accurately translated to other locations on the body, such as the finger pad [13]. Furthermore, these studies have primarily looked at area versus displacement, with the implicit assumption that the number of mechanoreceptors stimulated by a probe is a linear function of contact area. The relationship is in fact non-linear as a result of overlapping receptive fields and the finite number of mechanoreceptors on the finger[19]. Even a small point will contact a large number of receptors, and increasing the diameter of that point from $0.5mm$ to $2mm$ has almost no effect on the number of receptors stimulated. Similarly, because of the finite size of the fingerpad, decreasing

the tactile devices diameter from the full width of the fingerpad to a diameter approximately four millimeters smaller should stimulate nearly the same number of tactile receptors, albeit at the edge of their receptive fields. These factors must be considered if total skin stimulus is to be properly quantified.

Even significant stimulus can be hamstrung by time lag. Perceived latency between an event and the onset of vibrotactile stimulus can degrade the quality of feedback, but only begins to make an impact on user error rates beyond 25ms, and is not significantly perceptable until the lag reaches 50 ms [9, 2]. Therefore, in circumstances where user error is unacceptable, design of an impedance adapter should result in effective latencies of less than 25 ms. Likewise, in circumstances where some user error is acceptable, but perception of lag is not, latency should be constrained to within 50 ms. The addition of a transmission medium has the capacity to increase latency by delaying the signal from the motor and the success of the impedance adapter requires that it not increase latency beyond thresholds for error rate. As I investigate how a transmission medium can match a signal to the impedance of the skin, I will give special attention to delays in time to perception.

The design of high bandwidth low-profile tactile feedback systems demands optimization with respect to user perception of tactile sensation. Maximizing skin stimulus requires balancing skin indentation with stimulation of a large number of receptors. No known previous work has quantified the optimal balance between indentation and the number of receptors stimulated, an important component in the engineering of high-performance tactile systems. Herein, I endeavor to simulate the response of the human fingerpad to vibration, and use this simulation to find an optimal balance between depth of indentation and contact area.

Finally, simulation results were used to design and build functional prototypes. These prototypes were evaluated empirically with eight human subjects. The results show a significant decrease in power consumption, and a four-fold increase in skin displacement. Furthermore, results demonstrate that the system can generate vibration on the skin that is perceptually equivalent to a system without an impedance adapter at half the power – thus

increasing the range of haptic sensation in small, wearable devices.

This work's contribution is four-fold. I present:

1. A mathematically optimized model of an impedance adapter tuned to deliver energy to the skin.

2. A means of characterizing skin stimulation using depth of indentation and an estimate of the number of afferent nerve endings affected.

3. A physical prototype of an impedance adapter informed by the model.

4. An empirical evaluation of the device quantifying skin displacement and the perceived haptic sensation.

This work was done in conjunction with Blake Hannaford, Richard Adams, Iris Jiang, Shwetak Patel, and Eric Larson. Each of these people made a substantial contribution to the work documented here, whether through the generation of ideas, guidance on model development and testing, management of human subjects, or editing support. I was personally responsible for the testing of different vibrotactile motors, optimization of the impedance adapter, development of the skin model, experimental analysis of the linear resonant actuator, conception and development of the model of skin stimulus, optimization for skin stimulus, design and construction of the mechanical prototypes, conception of the empirical testing procedures, empirical testing for skin displacement, and analysis of all empirical data. I was also responsible for the bulk of the data analysis from simulation and the structure of the publications resulting from this work.

1.1 Theory of Operation

In typical operation, vibration motors supply energy to the skin by producing waves of force directly at the skins surface. These waves interact with the impedance of the skin, and are either absorbed into the skin through damping or reflected back off. In existing systems, the skins impedance is such that large amounts of the energy from the motor are actually reflected backwards and lost, and therefore do not contribute to perception.

The impedance adapter works as a matching network that takes the waves of vibration

from the motor and conditions them to match the impedance of the skin. The matching network consists of a coil-spring and steel dowels providing mass. This greatly reduces energy reflection, increasing energy absorption and resulting in greater perception. Tuning this matching network properly required constructing a mathematical model of the complete system, and adjusting the parameters of the impedance adapter to produce peak skin displacement.

Chapter 2

SIMULATION AND OPTIMIZATION

In the first phase of this work the impedance adapter was modeled mathematically and fed into a simulation. Before starting this work, there was limited evidence of the impact an impedance adapter might make on the coupling of energy between the motor and the skin; simulation was used to evaluate the potential of a properly tuned impedance adapter to improve energy transfer. The simulation was used to test different parameters for the impedance adapter, and a brute force optimization was used to select the best. The results formed the basis for the design of a prototype system, described in chapter 3.

2.1 Methods

2.1.1 Model

A mechanical model of the complete system comprising the LRA, impedance adapter, and finger was built using the standard system diagram approach (Figure 2.1). The modeling of the actuator came directly from analysis of the components of a C10-100 LRA (Precision Micro Drives[8], London, UK). The finger model is based on analysis of the literature reviewed in table 2.1. The impedance adapter is idealized as two masses, one connected to the LRA, the other to the skin, with a spring and damper between them.

The impedance adapter is modeled by four parameters, M_{a1}, M_{a2}, K_a, and B_a, describing the mass attached to the LRA, the mass attached to the skin, the spring between these two masses, and the damping between these two masses, respectively. The skin is modeled by a stiffness, K_s, and a damping, B_s. Contact area, A, governs changes in the skin impedance as described above.

This model produces the following equations of motion:

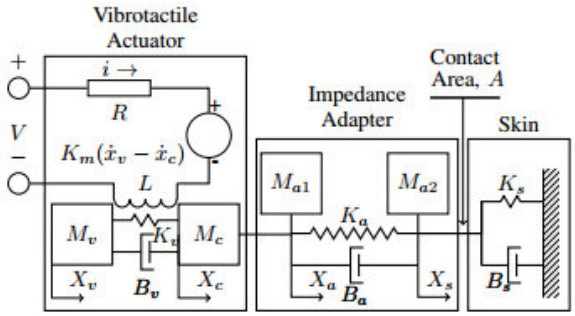

Figure 2.1: Dynamic model of vibrotactile actuator coupled to skin with an impedance adapter. Skin parameters depend on many variables including contact area (see text).

$$L\dot{i} + iR + K_m(\dot{x}_a - \dot{x}_v) = v(t) \tag{2.1}$$

$$M_v\ddot{x}_v + B_v(\dot{x}_v - \dot{x}_a) + K_v(x_v - x_a) = -K_m i \tag{2.2}$$

$$\begin{aligned}(M_c + M_{a1})\ddot{x}_a + B_v(\dot{x}_a - \dot{x}_v) + B_a(\dot{x}_a - \dot{x}_s) \\ + K_v(x_a - x_v) + K_a(x_a - x_s) = 0\end{aligned} \tag{2.3}$$

$$M_{a2}\ddot{x}_s + B_a(\dot{x}_s - \dot{x}_a) + K_A(x_s - x_a) + K_s x_s + B_s\dot{x}_s = 0 \tag{2.4}$$

These equations of motion produce the following linear first-order system of equations of the form $\dot{x} = Ax + Bu$ where

$$A = \begin{bmatrix} \frac{-R}{L} & 0 & \frac{K_m}{L} & 0 & \frac{-K_m}{L} & 0 & 0 \\ 0 & 0 & 1 & 0 & 0 & 0 & 0 \\ \frac{-K_m}{M_v} & \frac{-K_v}{M_v} & \frac{-B_v}{M_v} & \frac{K_v}{M_v} & \frac{B_v}{M_v} & 0 & 0 \\ 0 & 0 & 0 & 0 & 1 & 0 & 0 \\ \frac{K_m}{M_{cl}} & \frac{K_v}{M_{cl}} & \frac{B_v}{M_{cl}} & \frac{-(K_a+K_v)}{M_{cl}} & \frac{-(B_a+B_v)}{M_{cl}} & \frac{K_a}{M_{cl}} & \frac{B_a}{M_{cl}} \\ 0 & 0 & 0 & 0 & 0 & 0 & 1 \\ 0 & 0 & 0 & \frac{K_a}{M_{a2}} & \frac{B_a}{M_{a2}} & \frac{-(K_a+K_s)}{M_{a2}} & \frac{-(B_a+B_s)}{M_{a2}} \end{bmatrix} \tag{2.5}$$

$$x = \begin{bmatrix} i & x_v & \dot{x}_v & x_a & \dot{x}_a & x_s & \dot{x}_s \end{bmatrix}^T, \tag{2.6}$$

$M_{c1} = M_c + M_{a1}$, $B = [1/L, 0, 0, 0, 0, 0, 0]^T$, and $u = [V_{in}, 0, 0, 0, 0, 0, 0]^T$.

The csim() utility in Scilab[16] was used to simulate the time response of this system to sinusoidal inputs. The input to the system had an amplitude of 5V (10V peak-to-peak) and a frequency of 225Hz. For the purposes of this investigation we focused on the steady state root-mean-squared (RMS) value of x_s, the displacement of the skin. M_{a1}, M_{a2}, K_a, and B_a, and contact area, A, were then optimized (by a numeric search described below) to maximize steady state RMS skin displacement.

Parameters for the system (Table 2.1) were chosen based on values in the literature or the relevant manufacturer's data sheet [8] and verified by experiment where possible. Masses were found by disassembling a device and weighing its components. The resistance was measured using a multimeter. The elasticity, damping, and motor constant of the LRA were derived from its impulse response, which was measured by dropping the LRA and recording its voltage output response on an oscilloscope. Parameters were identified by fitting a damped exponential function with complex poles to this response constrained by the otherwise known values of mass, M_v, M_c, and resistance, R. Parameters for the impedance adapter were tuned through a numerical search and will be discussed in the results section.

To simulate the finger we chose to set a minimum value of skin stiffness at $600N/m$ and a maximum at $2000N/m$, both well within the reported range, and specific skin stiffness

Parameter	Value	Source
L	$130uH$	C10-100 Actuator Datasheet
R	27Ω	Measured, Data Sheet
M_v	$1.4g$	Measured, Data Sheet
M_c	$0.6g$	Measured, Data Sheet
B_v	$0.0322Nsec/m$	Experiment
K_v	$2800N/m$	Experiment
K_m	$1.0N/A$	Experiment
K_s	600-$1200N/m$	[13, 12, 3, 21, 18, 17]
B_s	0.75-2.38 $Nsec/m$	[13, 12, 21]

Table 2.1: Model Parameters

was set as a function of a 1/3 power of contact area between those two extremes. Likewise, we set the minimum value for damping at 0.75 $Nsec/m$ and the maximum at 2.38 $Nsec/m$, values which lay within the reported range, and set specific damping as a function of a 1/3 power of area. Variation across the human population was not accounted for.

A brute force numerical search was performed over the four parameters of the impedance adapter (M_{a1}, M_{a2}, K_a, B_a and A) to find the greatest steady state RMS skin displacement for a fixed input. Ranges for each parameter (Table 2.2) were established through a preliminary study that quantified the impact of individual parameter variations on system response. Parameters were then assigned limited ranges in which their impact on performance was non-negligible. In some cases the search returned results at either end of the range, indicating that an optimum may lie outside an achievable value. In these circumstances ranges were adjusted within physical limitations of the basic design. For instance, contact area was constrained to an upper bound the approximate size of the fingerpad and a lower bound designed to prevent skin puncture with a sharp, needle-like area. Likewise, masses were kept above 10 percent of the motor's mass to ensure they were manufacturable, and damping

Parameter		Parameter Search Range
M_{a1}	Mass attached to motor case	0.25 - 10.0g
M_{a2}	Mass attached to skin	0.25 - 10.0g
K_a	Impedance adapter spring	2000 - 12000 N/m
B_a	Impedance adapter damping	0.01 - 0.1 $Nsec/M$
A	Contact area	1 - 100 mm^2

Table 2.2: Parameter search ranges for the impedance adapter parameters.

was constrained to a minimum value of $0.01Ns/m$ because it cannot be entirely eliminated from physical designs. Each parameter was given 20 values within its search range.

The final performance measure we consider is skin stimulus. Evaluating skin stimulus requires an understanding of how increasing the depth of indentation and the number of mechancoreceptors stimulated impacts afferent nerve response. Mechanoreceptor response has a non-linear dependance on depth of indentation [7], and psychophysical sensation is non-linear as well, though the non-linearites do not appear to be correlated [19]. Importantly, both the mechanoreceptor response and psychophysical sensation appear to be linear at low indentations ($< 0.5mm$) [19]. Therefore stimulation can be considered proportional to indentation at small amplitudes. Furthermore, the responses of a population of receptors is additive [7]. Thus a representative skin stimulus parameter, S, can be defined as:

$$S = N_r \times x_{sRMS} \tag{2.7}$$

where N_r is the number of receptors and x_{sRMS} is the depth of skin indentation. Both the number of receptors stimulated and the depth of indentation are functions of contact area. Increasing contact area increases the number of receptors a device will directly stimulate. At the same time, for a constant input, increasing contact area reduces the depth of indentation. Therefore Eqn. 2.7 can be used to find the approximately optimal contact area to deliver vibrotactile stimulus to the fingerpad.

Contact condition	Area	x_{sRMS}
LRA direct	$78.5mm^2$	0.0438mm
LRA with cone	$1.0mm^2$	0.0455mm
LRA with Impedance Adapter	$1.0mm^2$	0.1917mm

Table 2.3: Steady state RMS displacement with sinusoidal 5V input under three contact conditions.

To determine the number of receptors directly stimulated by a device, the receptive fields on the fingerpad are modeled by a grid of overlapping circles whose radii define the receptive fields. The fingerpad is populated by four different types of mechanoreceptors; however, only fast acting type 2 (FAII) receptors are highly receptive to vibrations around 250Hz [19]. Valbo and Johansson found FAII mechnoreceptors to have receptive fields of approximately 101 mm^2. Thus $5.7mm$ was used as the radius for the receptive fields. FAII receptors have an innervation density of approximately $0.22/mm^2$ on the fingerpad[19]; this was the density used in simulation. Coupling this data with a model of a human fingerpad that is $15mm \times 15mm$ produces a grid of overlapping circles with $5.7mm$ radii across a space $15mm \times 15mm$. Simulated contactors with radii from $1mm$ to $7.5mm$ were then placed in the center of this system and the number of FAII receptive fields contacted for each contactor radius was recorded. This provided a measure of the number of FAII receptors directly stimulated over a range of contact areas. [4] found that additional mechanoreceptors can be stimulated by waves propogating through the body; careful analysis of the magnitude of these distant vibrations is beyond the scope of this paper. I submit this current means of measuring skin stimulus as an approximate measure.

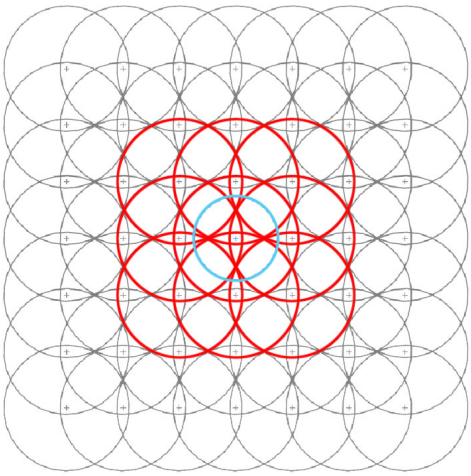

Figure 2.2: Receptive fields on the fingerpad. The blue cicle represents a contactor of radius 2, the red circles represent those receptors directly stimulated, and the grey circles are those unaffected.

2.2 Simulation Results

2.2.1 Initial Simulation

First, the model was simulated without an impedance adapter present. There are two relevant cases. One, the LRA can be applied directly in contact with the skin. The device we used had a surface area of $78.5mm^2$ which was thus a fixed parameter in the model. The resulting steady state RMS displacement was $0.0438mm$ (Table 2.3). Two, a rigid massless cone could be placed between the LRA and the skin, reducing the stimulation area to 1 mm^2. In this case, the resulting steady state RMS displacement was $0.0455mm$

When driven by the 10V peak-to-peak sinusoid described above, the current and power computed at the electrical input were 130 mA and 457 mW in the steady state. The phase angle between voltage and current was 0.1 degrees.

2.2.2 Optimization for skin displacement

The numerical search described above produced parameters that maximized steady state RMS skin displacement in response to the sinusoidal +/-5V input to the LRA. The process yielded a steady state RMS skin displacement 4.4 times larger than the displacement without an impedance adapter, and reduced RMS current consumption and power by 15%. A plot of skin displacement over time for both the system with an impedance adapter and without are shown in Figure 2.3. The parameters of the optimized impedance adapter are shown in Table 2.3.

The approach works by matching the impedance of the skin to the impedance of the motor. If the impedance adapter has achieved this impedance match, the impedance at the interface of the skin and the adapter should be very nearly equal at the operating frequency (in this case 220 Hz). Figure 2.4 shows the frequency response of the impedance of the skin and the impedance of the LRA + impedance adapter, and demonstrates that the optimized parameters produce a match.

Some of these parameters proved to be sensitive to small changes, while others were more robust. In particular, changes made to the mass attached to the skin (M_{a2}), the impedance adapter stiffness (K_a), and the skin damping (B_s) resulted in large changes in the steady state RMS displacement of the skin (Figure 2.5). Parameters not shown (M_{a1}, B_a, and K_s) impacted the output by less than 2 percent when varied by up to 50 percent.

2.2.3 Skin Stimulus

By geometric analysis, we computed the number of mechanoreceptors stimulated as a function of contactor area (Figure 2.6). These data were then combined with results from the LRA-Impedance adapter model, which supplied the steady state RMS depth of indentation for contactors of any given area. The two sets of data were combined according to Equation 2.7, and the results are plotted below in Figure 2.7. The maximum skin stimulus possible with an impedance adapter was 4.90, while the maximum stimulus without an adapter was

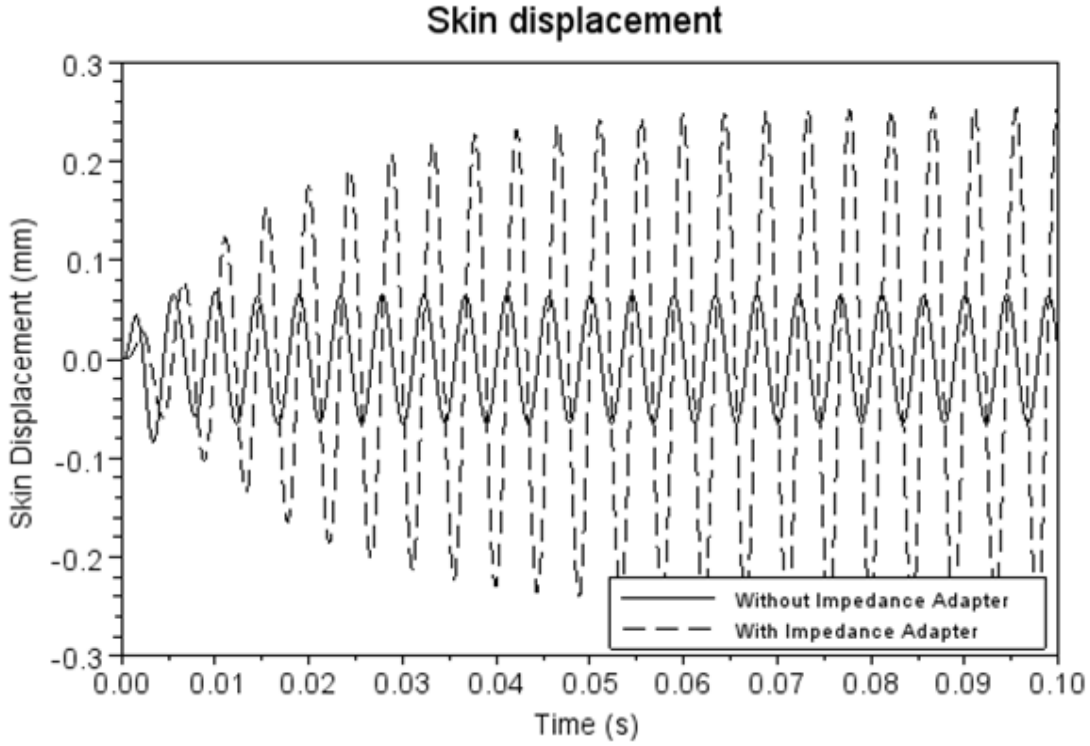

Figure 2.3: Simulated skin displacement over time. The system with an impedance adapter has a much longer rise time, but achieves an amplitude approximately four times greater than the system without.

Parameter		Optimal value
M_{a1}	Mass attached to motor case*	$0.25g$
M_{a2}	Mass attached to skin	$4.35g$
K_a	Impedance adapter spring	$8200N/m$
B_a	Impedance adapter dampin*g	$0.01Nsec/M$
A	Contact area*	$1.0mm^2$
ω_d	Resonant frequency	$218Hz$

Table 2.4: Optimized impedance adapter parameters. Values marked with * were saturated at their lower search bound.

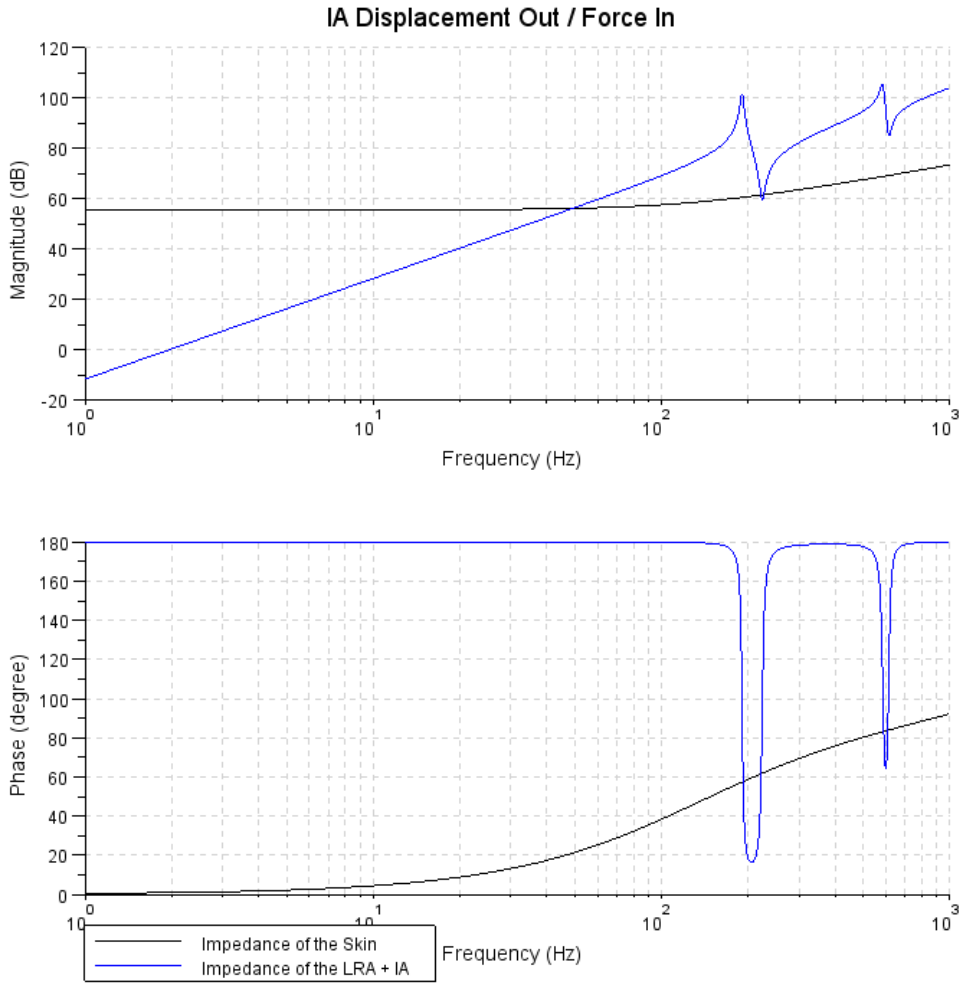

Figure 2.4: Impedance of the skin and impedance of the LRA + impedance adapter over a range of frequencies. The impedance adapter creates a dip in impedance right at the operating frequency, matching the impedance of the skin.

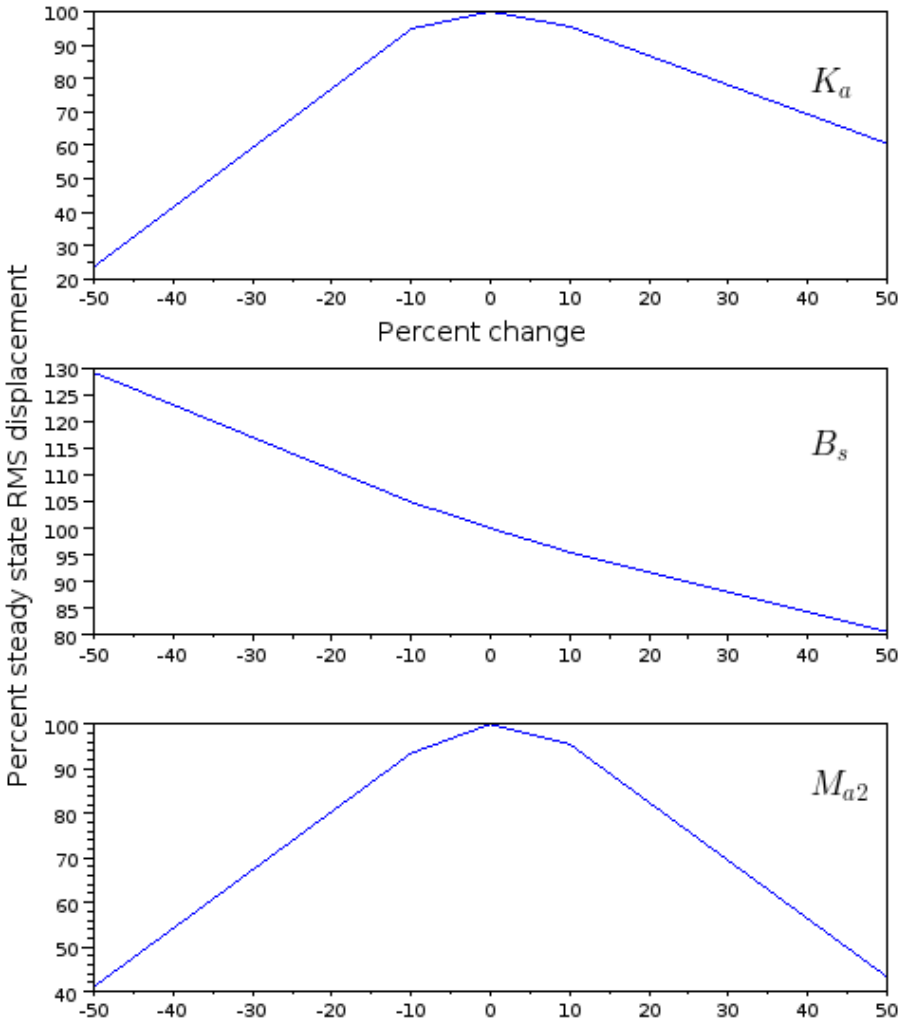

Figure 2.5: Sensitivity of RMS displacement output to changes in the impedance adapter and the skin model parameters. K_a impedance adapter stiffness; B_s skin damping; M_{a2} mass at skin contact. X-axis: percent change from optimal parameter value, Y-axis: relative steady state RMS displacement.

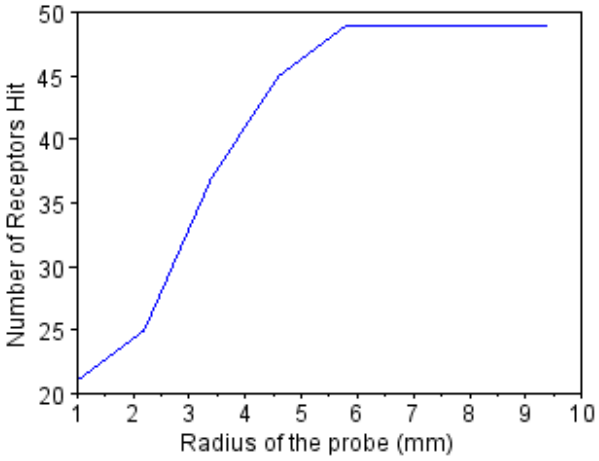

Figure 2.6: Number of receptors stimulated (N_r) as a function of contactor area.

2.15 (both in units of $mm \times N_r$). The system with an impedance adapter achieved greater than twice the stimulus of the system without.

2.3 Simulation Discussion

Our simulations of a vibrotactile actuator, impedance adapter, and skin showed that an impedance adapter could increase the steady state RMS displacement of the skin by a factor of 4.4, and the total skin stimulus by a factor of 2.3. These improvements reflect the increased transmission of energy from the actuator through the skin, facilitated by the mechanical properties of the impedance adapter. The presence of a tuned impedance adapter improves signal transmission, increasing energy input to the skin while simultaneously decreasing energy consumed by the motor. These results show the potential of an impedance adapter to improve haptic feedback and lower power consumption in haptic devices.

The simulation of receptor fields (Figures 2.2, 2.6, and 2.7) did not account for the gradual drop off in the receptive field of FAII type mechanoreceptors, and simply used the average field size given in the literature for the human fingerpad [19]. It is not known exactly how far these fields extend, and they appear to be subject to great variability[19]. We

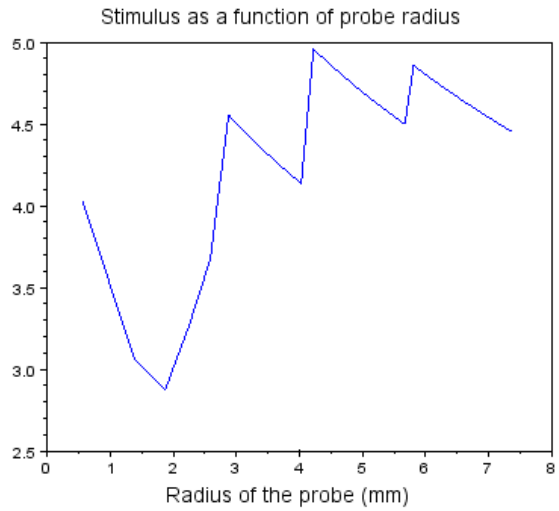

Figure 2.7: Skin Stimulus as a function of contactor radius. The rough contours of the graph are an artifact of simulation due to a simplified distribution of skin receptors.

restricted our model to be within the demonstrated range of these receptors, and produced a conservative estimate. This platonic model simulated a finger where all the receptors are evenly spaced, and all have an equally large fields with sharp edges. The sharp changes in stimulation depicted in Figure 2.7 occur when the increased radius makes it just barely possible to reach the edge of a receptors receptive field. In reality I would expect more gradual shifts in skin stimulus owing to the variable distribution of receptors and receptive fields which drop off slowly, thus smoothing the jagged edges in Figure 2.7. Nevertheless, the results highlight a trade-off between smaller indentation and increased quantity of receptors stimulated as probe size is increased.

Conflicting reports in the literature make it difficult to develop a model of the human fingerpad that could be said to be accurate for all people in all cases. Furthermore, between subjects variation was great enough in some studies to substantially influence the absolute amplitude of vibration found in the model [21]. Better models of the skin's mechanical properties over a range of factors such as contact area and depth of indentation will help refine this work, and are necessary to ground the results of the simulation in the real world.

Nonetheless, the model can provide concrete information on the design of a real-world impedance adapter. For example, the model supports the existance of an optimum value for impedance adapter stiffness and showed that damping in the impedance adapter should always be minimized.

The optimization set a lower limit on contact area, damping, and M_{a1} at 1 mm^2, 0.01 Ns/m, and 0.25 g, respectively. As Table 2 makes clear, these were also their final optimized values. If unconstrained, these values would go to zero. Damping is a measure of energy the system can absorb. In this case, the system is trying to maximize energy transmission, so lowering the damping makes sense. Likewise, contact area was used in a 1/3 power law to find skin stiffness and damping. As contact area shrinks, so does skin stiffness and damping, both factors which impede contactor displacement. Therefore it makes sense for the optimization to shrink these values to their minimum.

The mass attached to the LRA, M_{a1}, is the third variable driven to zero in the numerical search. In parametric analysis where the value of M_{a1} is varied while all other parameters were held constant, its effect on steady state displacement is almost non-existent when it remains below 2 grams. Beyond this point it seems to cause a steady decrease in steady state displacement until it reaches 25 grams, the limit of the test. These tests show that decreasing M_{a1} below 2 grams results in marginal increases in displacement. Should a constraint such as manufactuability require M_{a1} to be an order of magnitude greater than the optimium value, the performance penalty will be small.

The introduction of an impedance adapter did not increase the latency of the system. As figure 2.3 shows, both systems followed the same curve at the start of the stimulus, and there was no point when the system without an impedance adapter produced a larger displacement. Thus the system with an impedance adapter had an equivalent time to perception. To the extent the model is linear, an input voltage one third the size will produce an output displacement one third as large. This opens the door to very low power vibrotactile systems which use an impedance adapter to achieve equivalent displacement while cutting power. However, these systems may face a much greater latency as a system with

an impedance adapter has a much longer rise time than a system without.

Furthermore, these systems may suffer from non-linear effects in the skin, the motor, and the mode of operation. As previously discussed, the dynamics of the skin are highly non-linear. I have attempted to include some non-linearity into our model by defining the skin parameters as a function of a 1/3 power law of area, and avoid other areas of non-linearity by indenting the skin by only a few hundred microns, but these fixes do not insulate the model from error in the skin mechanics. Likewise, the system does not capture the real-world non-linearity of the LRA, which has travel limits on its moving mass and a spring that is likely to be non-linear near those limits. Finally, the model does not account for discontinous contact between the impedance adapter and the skin. These effects are sure to play a role, and required experimental verification.

Chapter 3

PROTOTYPING AND EXPERIMENTAL VALIDATION

Two prototypes were created with different contact areas as simulation results indicate that maximum displacement is achieved using a contact area of 1 mm^2, while maximum sensation was achieved using a contact area of 64 mm^2. Both impedance adapters include a Precision Microdrives C-10 linear resonant actuator (LRA), a steel compression spring, a plastic base, steel dowel pins, and elastic band 1.25cm wide (see Figure 3.1). The steel compression spring was cut to length from stock, and its new spring constant was measured. The plastic base was 3D printed and included a mount for the dowel pins, spring, and elastic band. Furthermore, the base had a carefully measured area in contact with the skin. Impedance adapter 1 (IA#1) had a contact area of 64 mm^2 and impedance adapter 2 (IA#2) had a contact area of 1 mm^2. Both plastic bases were fitted with two dowel pins, and weighed 4.6g including the pins.

The complete assembly consisted of the LRA, spring, and base in series with the skin as shown in Figure 3.1. The elastic band was sewn to the base and wrapped around the finger.

Based on simulation results, I hypothesized that IA#1 would increase perceived sensation by a factor of 2.5 and IA#2 would produce a four-fold increase in skin displacement. The prototypes were tested with two experiments that evaluated (1) the skin displacement between an impedance adapter and a control and (2) the power requirements for the impedance adapters to provide equivalent perceived sensation as compared to a vibrotactile control.

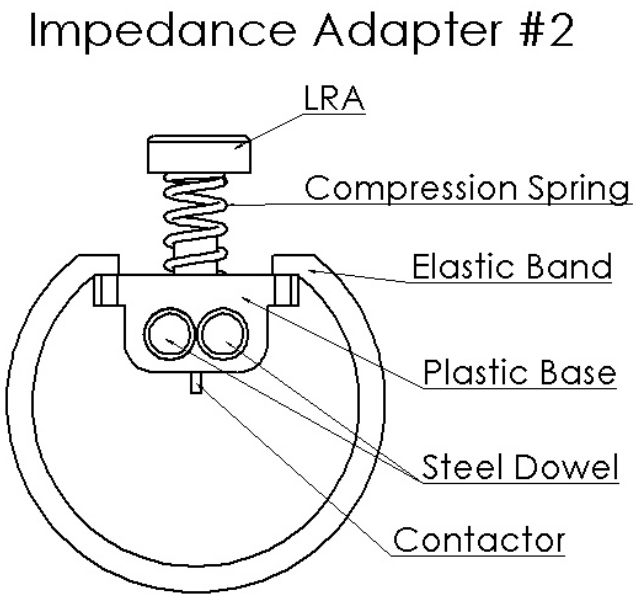

Figure 3.1: Schematic diagram of an impedance adapter and LRA. The finger is placed through the loop of the elastic band.

3.1 Skin Displacement

In this evaluation I measured the movement of the skin in response to the motor with and without the impedance adapter. Skin displacement was measured using a Keyence IL-030 laser distance sensor, which provides a resolution of 0.001*mm*.

3.1.1 Experiment

In the control condition the laser was focused on the top of the LRA, with the finger directly in contact with the LRA. The finger was assumed to be in constant contact with the LRA. When the impedance adapter was present, the laser was focused on the plastic base sitting directly on the skin. The base was again assumed to be in constant contact with the skin. The base was thick enough that any flex was assumed to be small in comparison to the oscillation of the system, see Figure 3.2.

In all conditions, the vibrating system was held in contact with the skin using an elastic band. The elastic was sized to loosely hold the system in place, and designed to minimize static pressure against the fingerpad. Paper shims were used to ensure the oversized band fit evenly across participants. The band experienced very little stretch when properly shimmed, and most of the static pressure on the skin was a result of the weight of the impedance adapter and LRA.

With a total mass of 7.5g the impedance adapter system produced a gravitational force on the finger of 0.06N, resulting in a displacement of $0.75mm$. However, this displacement should not affect the properties of the finger – other studies have found that this level of static pressure has a minimal effect on the mechanical impedance of the fingertip [13]. Furthermore, work by Lamore and Keemink found no difference in the vibrotactile threshold at high frequencies between static loading conditions [11]. Thus the gravitational force should have no effect on the experiments.

Skin displacement was measured using a stock LRA, an LRA with a 1.1 mm^2 contact area, and both impedance adapters. Eight subjects (four female, four male) were tested in all four conditions, three trials per condition. All tests were conducted using the participants index finger. The study was approved by the University of Washington Human Subjects Division, approval #44695. The data from the distance sensor were band-pass filtered in the frequency range of interest (20-500Hz) to remove hand tremor and high frequency noise. I then calculated the root-mean-square (RMS) skin displacement for each trial using the filtered data.

3.1.2 Results

IA#1 and IA#2 were able to significantly increase skin displacement as compared to a stock LRA by a factor of 3.26 and 4.25 on average, respectively (based on a paired t-test, p¡0.001). The mean RMS displacement and standard deviation for all conditions is shown below in figure 3.3.

Figure 3.2: The prototype impedance adapter in test setup for displacement measurement.

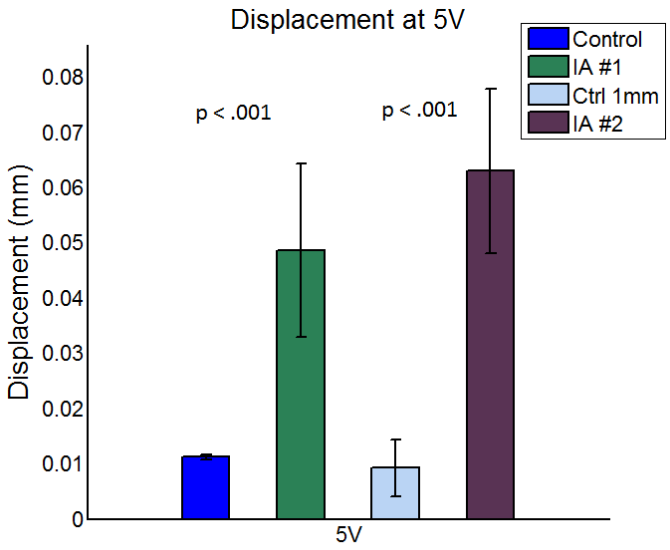

Figure 3.3: (A) RMS skin displacement for a contactor with a radius of 4.5*mm*. (B) RMS skin displacement for a contactor with a radius of 1*mm*

3.2 Equivalent Perception

All eight subjects also participated in a perceptual equivalence test. Each subject wore the stock LRA on their right index finger. This was used as the reference. On the left index finger, subjects wore one of the four test conditions: a stock LRA, an LRA with 1.1mm^2 contact area, IA#1, or IA#2. Subjects were instructed to try and match the vibration level felt on the left finger with the vibration felt on the reference finger.

3.2.1 Experiment

The motors were driven by two separate power supplies. The experimenter would set the voltage of the reference motor to 1 of 5 settings (1V, 2V, 3V, 4V, or 5V), and provide 1s bursts of vibration to both motors at the same time. Both motors vibrated at a constant frequency of 175Hz. Subjects would tell the experimenter whether they felt the voltage of the test motor should be higher or lower, and the experimenter would adjust the voltage

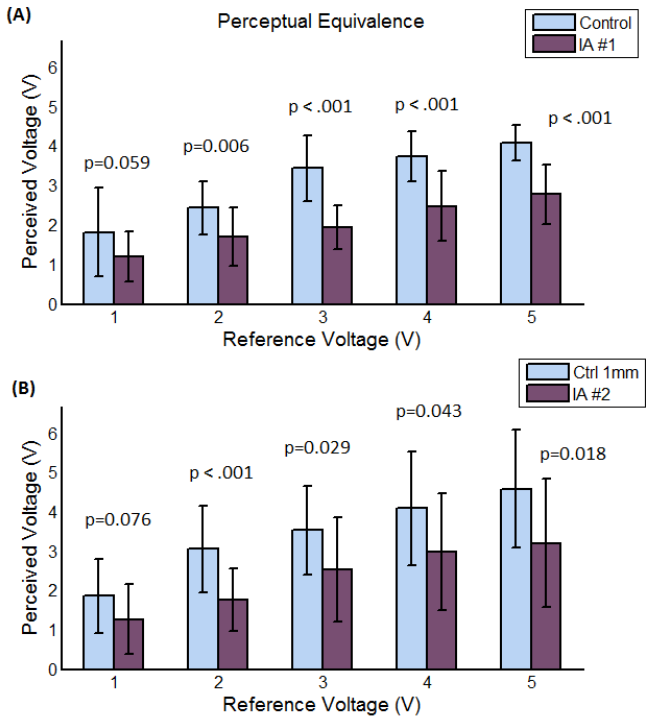

Figure 3.4: Subjects adjust voltage levels on an LRA on one index finger to match the vibration sensed from an LRA on the other index finger. (A) Shows tests with a large radius, (B) shows tests with a smaller radius.

of the test motor until the subject perceived both motors to feel the same. Subjects wore earmuffs to block the sound of the vibration and were positioned so they could not see the voltage readings on the power supplies. Each of the four test conditions was presented in random order. Each voltage level within a test condition was also presented in a random order. Each test consisted of 10 trials (2 trials per voltage level).

3.2.2 Results

The results of the perceptual equivalence study are shown in figure 4. Figure 4 (A) compares IA#1 to the LRA with the same $64mm^2$ contact area. Figure 4 (B) compares IA#2 to the LRA with the same $1mm^2$ contact area. The results show that subjects set the test volt-

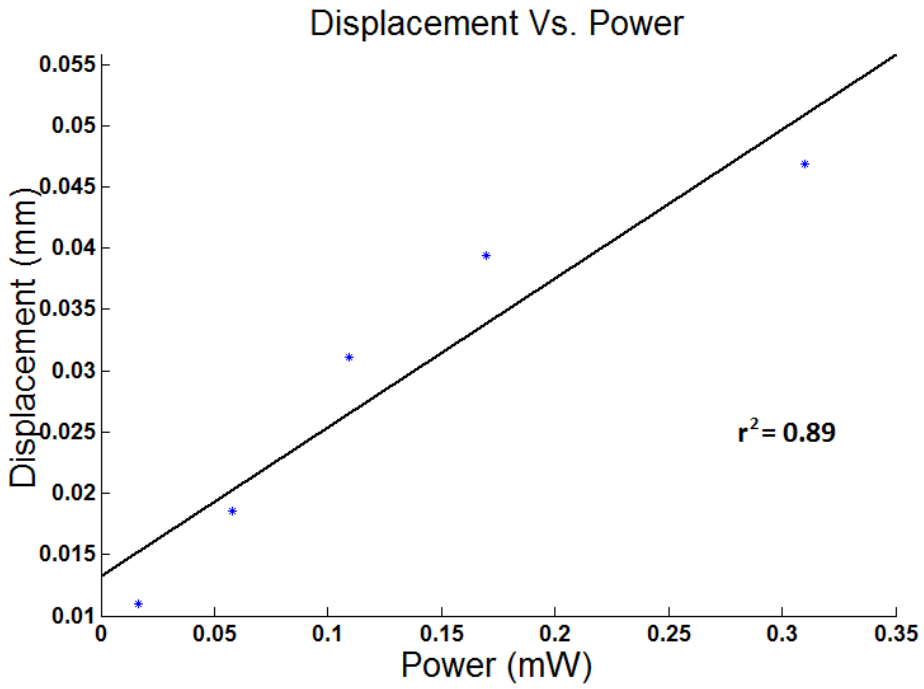

Figure 3.5: Linearity of the LRA and impedance adapter at power levels.

age 35% lower on average for IA#1 and 32% lower on average for IA#2 than the reference voltage applied to a stock LRA. There was no statistically significant difference between the reference voltages and the test voltages for either control condition. Subjects evaluation of equivalent voltage settings varied between low reference voltages and high reference voltages. With a 1V reference, it was not clear whether subjects could distinguish between a system with an impedance adapter and a system without. In both conditions, however, subjects could distinguish between the two systems when the reference voltage was 2V or higher, and subjects applied a significantly lower voltage to the system with an impedance adapter ($p < 0.05$).

3.3 Discussion

Simulations expected IA#2 to out-perform the stock LRA by a factor of 4.40, which is remarkably close to the empirical finding of a 4.25x improvement. IA#1 fared even better

than simulation, with an expected improvement of 2.28x and a measured improvement of 3.26x. This demonstrates an error in the model, and suggests that mechanical stiffness and damping do not increase as a 1/3 power law of contact area.

In the perceptual equivalence study, the voltage for the system with an impedance adapter was consistently set at approximately 66% of the voltage for the system without an impedance adapter. This suggests that an impedance adapter can be used to lower power consumption by 55%. Even so, this is a lower percentage than might be expected based on psychophysical tests by [1], who found a linear relationship between depth of indentation and stimulation. This suggests that the four-fold increase in skin displacement should have resulted in a 75% drop in equivalent power, given a linear relationship between power and displacement.

This difference could be attributed to subjects inability to discriminate between small changes in voltage level. For instance, when adjusting voltage levels to be equivalent, if the voltage was initially low, the subject would generally say to stop adjusting the voltage at a lower level. If the voltage was initially set high, then the subject would say to stop at a higher voltage. Thus, equivalence in our experiments may be artificially high – the true equivalence level for minimizing the power could be ascertained by always adjusting the voltage level up from a lower voltage.

However, the difference could also be attributed to non-linear dynamics in the LRA and impedance adapter at low power levels. To test this latter hypothesis, two subjects participated in a skin displacement test using IA#1 as input voltage was swept from 1V to 5V. The results are shown in Figure 3.5, illustrating a linear relationship between power and displacement. Thus, the discrepancy in theorized power reduction and actual power reduction is not due to non-linearity in the LRA. It is more likely due to the resolution at which subjects could perceive the vibrotactile sensation. Therefore we believe these results show a worst case power reduction. The possible power savings are likely much greater than 55% (and might be as high as the theorized 75%).

Chapter 4

CONCLUSION

This paper demonstrates that an optimized mass-spring-damper, dubbed an impedance adapter, placed between a vibrational actuator and the human skin can potentially increase skin displacement, and thus the magnitude of the resulting haptic stimulus. An impedance adapter provides a means to significantly improve haptic feedback by matching the impedance of the signal to the impedance of the source. Simulations based on a commonly available linear resonant actuator (LRA) demonstrate that such a device could increase skin displacement by a factor of four, and double skin stimulation. Empirical testing of our prototype impedance adapters has demonstrated the significant improvement they offer over a typical system. Results were in line with expectations from simulation, though they do suggest some adjustment of the skin model. The current working prototype is significantly larger than a typical vibration motor, failing the goal to reduce system size. However, the entire system is based on the parameters of the model, and could be great shrunk by using dense materials for the mass and softer materials for the spring.

4.1 Future Work

Though the system was designed and tested for use on an idealized fingerpad, it was remarkably robust to variations in the skin that naturally occur across users. This points to potential to use the same system on parts of the body for which it was not designed. Future work could explore the resilence of the system to more significant changes in skin biomechanics by testing the device on the palm, the arm, the leg, or other interesting sites. Furthermore, improvements in the understanding of traveling vibrotactile waves could help to improve the optimization of skin stimulus, and should be explored. The impact of these

waves could be tested using a mechanical surround to damped vibrations outside the area of interest. In addition to the insight this might provide into the psychophyiscal effects of travelling waves, it could allow for more focused delivery vibrotactile stimulus.

One major shortcoming in the model is the lack of a ground for the motor. While the prototype allowed the motor to vibrate freely, systems like mobile devices, space suits, and haptic controllers would likely ground the motor and maintain skin contact through a user's grip. Redefining the model with new constraints might produce a very different optimum, with valuable results for integration into larger devices.

It's worth noting that the optimization did not optimize for power transfer, but for skin displacement. This was grounded in psychophysical results demonstrating a strong correlation between skin displacement and sensation. However, exploring the difference in sensation produced by a system optimized for power transfer instead of skin displacement might yield insight into psychophysical mechanisms for vibrotactile sensation. To my knowledge, no work has been done looking at the connection between power into the skin, given by force times velocity, and sensation.

The work described here used a simple linear second order model for the amplifier because such a model is straightforward to analyze and implement. However, more nuanced models might yield better results. Non-linear amplifiers offer the potential to shift the frequency, giving designers the power to use vibration motors which operate at frequencies above or below the 250 Hz at which the skin is most sensitive, while still delivering stimulation in the most sensitive bands of frequency. Having demonstrated the potential to greatly improve stimulation with optimization, more advanced models become much more attractive.

Finally, there exists great potential to operative these amplifiers in reverse, amplifying ambient vibrations to power a generator. Such devices could give life to miniature, mobile devices with infinite life, and allow for a new realm of sensing far from a power grid. Such applications require significant future study, but are within the scope of a dissertation, and could have a major impact in the world of ubiquitous computing, health monitoring, and

structural sensing.

BIBLIOGRAPHY

[1] KR Hardick G A. Gescheider, SJ Bolanowski. The frequency selectivity of information-processing channels in the tactile sensory system. *Somatosensory & Motor Research*, 18(3):191–201, 2001.

[2] B.D. Adelstein, D.R. Begault, M.R. Anderson, and E.M. Wenzel. Sensitivity to haptic-audio asynchrony. *Proceedings of the 5th international conference on Multimodal interfaces*, pages 73–76, 2003.

[3] J. Biggs and M.A. Srinivasan. Tangential versus normal displacements of skin: Relative effectiveness for producing tactile sensations. *Haptic Interfaces for Virtual Environment and Teleoperator Systems, 2002. HAPTICS 2002. Proceedings. 10th Symposium on*, pages 121–128, 2002.

[4] B. Delhaye, V. Hayward, P. Lefèvre, and J.L. Thonnard. Texture-induced vibrations in the forearm during tactile exploration. *Frontiers in Behavioral Neuroscience*, 6, 2012.

[5] E.K. Franke. Mechanical impedance of the surface of the human body. *J. Appl. Physiology*, 3:582–590, 1951.

[6] M. Fritschi, K. Drewing, R. Zopf, M.O. Ernst, and M. Buss. Construction and first evaluation of a newly developed tactile shear force display. In *Proceedings of the 4th International Conference EuroHaptics 2004*, pages 508–511, 2004.

[7] A.W. Goodwin and H.E. Wheat. Physiological mechanisms of the receptor system. *Human Haptic Perception: Basics and Applications*, pages 93–102, 2008.

[8] Precision Micro Drives Inc. Website. *http://precisionmicrodrives.com*, 2012.

[9] C. Jay, M. Glencross, and R. Hubbold. Modeling the effects of delayed haptic and visual feedback in a collaborative virtual environment. *ACM Transactions on Computer-Human Interaction (TOCHI)*, 14(2):8, 2007.

[10] Iris Jiang, Yuki Ishikawa, Jack Lindsay, and Blake Hannaford. Design and optimization of support structures for tactile feedback.

[11] PJJ Lamoré and CJ Keemink. Evidence for different types of mechanoreceptors from measurements of the psychophysical threshold for vibrations under different stimulation conditions. *The Journal of the Acoustical Society of America*, 83:2339, 1988.

[12] R. Lundström. Local vibrationsmechanical impedance of the human hand's glabrous skin. *Journal of biomechanics*, 17(2):137–144, 1984.

[13] T.J. Moore and J.R. Mundie. Measurement of specific mechanical impedance of the skin: effects of static force, site of stimulation, area of probe, and presence of a surround. *The Journal of the Acoustical Society of America*, 52:577, 1972.

[14] B.J.P. Mortimer, G.A. Zets, and R.W. Cholewiak. Vibrotactile transduction and transducers. *The Journal of the Acoustical Society of America*, 121(5):2970–2977, 2007.

[15] DT Pawluk, R.D. Howe, et al. Dynamic lumped element response of the human fingerpad. *Journal of biomechanical engineering*, 121(2):178, 1999.

[16] Scilab. Website. *http://www.scilab.org*, 2012.

[17] ER Serina, CD Mote, and DM Rampel. Mechanical properties of the fingertip pulp under repeated, dynamic, compressive loading. volume 31, pages 245–246. AMERICAN SOCIETY OF MECHANICAL ENGINEERS, 1995.

[18] M.A. Srinivasan T.T. Diller, D. Schloerb. Frequency response of human skin in vivo to mechanical stimulation. Technical Report 648, MIT Research Laboratory of Electronics (RLE), Feb. 2001.

[19] Å.B. Vallbo, RS Johansson, et al. Properties of cutaneous mechanoreceptors in the human hand related to touch sensation. *Human neurobiology*, 3(1):3–14, 1984.

[20] R.T. Verrillo. Vibrotactile thresholds for hairy skin. *Journal of Experimental Psychology; Journal of Experimental Psychology*, 72(1):47, 1966.

[21] M. Wiertlewski and V. Hayward. Mechanical behavior of the fingertip in the range of frequencies and displacements relevant to touch. *Journal of biomechanics*, 45(11):1869–1874, 2012.

[22] John S Zelek, Sam Bromley, Daniel Asmar, and David Thompson. A haptic glove as a tactile-vision sensory substitution for wayfinding. *Journal of Visual Impairment and Blindness*, 97(10):621–632, 2003.